



HAL
open science

Normal and excess nitrogen uptake by iron-based Fe-Cr-Al alloys; the role of the Cr/Al atomic ratio
Kyung Sub Jung, Ralf Schacherl, Ewald Bischoff, Eric Jan Mittemeijer

► **To cite this version:**

Kyung Sub Jung, Ralf Schacherl, Ewald Bischoff, Eric Jan Mittemeijer. Normal and excess nitrogen uptake by iron-based Fe-Cr-Al alloys; the role of the Cr/Al atomic ratio. Philosophical Magazine, 2011, pp.1. 10.1080/14786435.2011.563760 . hal-00681620

HAL Id: hal-00681620

<https://hal.science/hal-00681620>

Submitted on 22 Mar 2012

HAL is a multi-disciplinary open access archive for the deposit and dissemination of scientific research documents, whether they are published or not. The documents may come from teaching and research institutions in France or abroad, or from public or private research centers.

L'archive ouverte pluridisciplinaire **HAL**, est destinée au dépôt et à la diffusion de documents scientifiques de niveau recherche, publiés ou non, émanant des établissements d'enseignement et de recherche français ou étrangers, des laboratoires publics ou privés.



Normal and excess nitrogen uptake by iron-based Fe-Cr-Al alloys; the role of the Cr/Al atomic ratio

Journal:	<i>Philosophical Magazine & Philosophical Magazine Letters</i>
Manuscript ID:	TPHM-10-Dec-0509
Journal Selection:	Philosophical Magazine
Date Submitted by the Author:	17-Dec-2010
Complete List of Authors:	Jung, Kyung Sub; Max Planck Institute for Metals Research, Prof. Dr Ir. E.J. Mittemeijer Schacherl, Ralf; Universität Stuttgart Bischoff, Ewald; Max Planck Institute for Metals Research, Prof. Dr Ir. E.J. Mittemeijer Mittemeijer, Eric Jan; Max Planck Institute for Metals Research, Prof. Dr Ir. E.J. Mittemeijer
Keywords:	surface treatments, nitrides, phase transformations
Keywords (user supplied):	gas nitriding, absorption isotherms, ternary alloy

SCHOLARONE™
Manuscripts

1
2
3 **Normal and excess nitrogen uptake by iron-based Fe-Cr-Al alloys;**
4
5 **the role of the Cr/Al atomic ratio**
6
7

8 K. S. Jung^{a,*}, R. E. Schacherl^b, E. Bischoff^a, E. J. Mittemeijer^{a,b}
9

10 ^a Max Planck Institute for Metals Research, Heisenbergstr. 3, D-70569 Stuttgart,
11
12 Germany
13

14 ^b Institute for Materials Science, University of Stuttgart, Stuttgart, Germany
15
16
17

18
19
20 * Corresponding author
21

22 K.S. Jung: k.s.jung@mf.mpg.de
23

24 Postal address: Max Planck Institute for Metals Research, Heisenbergstr. 3, D-
25
26 70569 Stuttgart, Germany
27

28
29 Tel: +49 711 689 3354
30

31 Fax: +49 711 689 3312
32
33
34
35

36 Co-authors
37

38 R.E. Schacherl: r.schacherl@mf.mpg.de
39

40 E. Bischoff: bischoff@mf.mpg.de
41
42

43 E.J. Mittemeijer: e.j.mittemeijer@mf.mpg.de
44
45
46
47
48
49
50
51
52
53
54
55
56
57
58
59
60

Abstract

Upon nitriding ferritic iron-based Fe-Cr-Al alloys, containing a total of 1.50at.% (Cr + Al) alloying elements, with varying Cr/Al atomic ratio (0.21 - 2.00), excess nitrogen uptake occurred, i.e. more nitrogen was incorporated in the specimens than compatible with only inner nitride formation and equilibrium nitrogen solubility of the unstrained ferrite matrix. The amount of excess nitrogen increased with decreasing Cr/Al atomic ratio. The microstructure of the nitrided zone was investigated by X-ray diffraction (XRD), electron probe microanalysis (EPMA), transmission electron microscopy (TEM) and electron energy loss spectroscopy (EELS). Metastable, fine platelet-type, mixed $\text{Cr}_{1-x}\text{Al}_x\text{N}$ nitride precipitates developed in the nitrided zone for all of the investigated specimens. The degree of coherency of the nitride precipitates with the surrounding ferrite matrix was discussed in view of the anisotropy of the misfit. Analysis of nitrogen-absorption isotherms, recorded after subsequent pre- and de-nitriding treatments allowed to differentiate quantitatively different types of nitrogen taken up. The amounts of the different types of excess nitrogen as function of the Cr/Al atomic ratio were discussed in terms of the nitride/matrix misfit and the different chemical affinities of Cr and Al for N. The strikingly different nitriding behaviors of Fe-Cr-Al and Fe-Cr-Ti alloys could be explained on this basis.

Keywords: gas nitriding, absorption isotherms, ternary alloy, excess nitrogen

1. Introduction

Nitriding is a thermochemical surface-treatment process of ferritic steel components in order to improve properties such as the resistances against fatigue, corrosion and wear [1-7]. In order to introduce nitrogen into the component, gaseous nitriding, employing NH_3 -based atmospheres, is widely adopted. The application of a NH_3/H_2 gas mixture, instead of pure N_2 gas, makes it possible to impose, at 1atm and in a temperature range of 500 - 580°C, at the surface of the specimen to be nitrided, a chemical potential of nitrogen equivalent to that of thousands of atmospheres of N_2 gas. To this end the slow thermal dissociation of NH_3 under these conditions is crucial [8, 9].

Upon nitriding of iron-based binary alloys containing alloying elements with a strong affinity for nitrogen, such as Cr [10-21], Al [22-27], V [28-33] and Ti [34-37], alloying element nitride precipitates can develop in the diffusion zone.

Chromium and aluminum are often used together as alloying elements (Me) in commercial nitriding steels. Only very recently a few studies were devoted to the nitriding of such ternary iron-based Fe-Me₁-Me₂ alloys. Whereas, upon nitriding, in binary Fe-Cr alloys rapid precipitation of highly coherent, cubic rock-salt crystal-structure type CrN nitrides takes place [12, 13, 16], in binary Fe-Al alloys hexagonal, wurtzite, crystal-structure type AlN nitrides precipitate with difficulty, i.e. only slowly [23-26]. It was shown that the total amount of nitrogen taken up per atom alloying element Me was rather different for Fe-Cr and Fe-Al alloys.

Recent research on a ternary iron-based Fe-Cr-Al alloy has shown that nitriding of such an alloy leads to the precipitation of metastable, mixed $\text{Cr}_{1-x}\text{Al}_x\text{N}$ nitride precipitates of cubic, rock-salt crystal-structure type [38]. Then, in view of the above discussed different nitriding effects of Cr and Al in binary Fe-Me

1
2
3 alloys, it is of interest to quantitatively investigate the uptake of nitrogen by Fe-
4
5 Cr-Al alloys, in particular as function of the Cr/Al atomic ratio, which is the
6
7 purpose of the present project.
8
9

10 Using homogeneously nitrated foils of Fe-Cr-Al alloys with different
11
12 Cr/Al atomic ratios ($0.21 \leq \text{Cr/Al} \leq 2.00$), while keeping the total amount of the
13
14 alloying element at about 1.50at.%, so-called nitrogen-absorption isotherms (cf.
15
16 section 3.4) were determined and discussed in terms of various types of absorbed
17
18 nitrogen. The microstructure of the nitride zone and the morphology and
19
20 composition of the nitride precipitates were investigated by means of X-ray
21
22 diffraction (XRD), electron probe microanalysis (EPMA), transmission electron
23
24 microscopy (TEM) and electron energy loss spectroscopy (EELS).
25
26
27
28
29
30

31 **2. Experimental**

32 **2.1 Specimen preparation**

33
34 Ingots of Fe-Cr-Al alloys, containing about 1.50at.% (Cr + Al), with the Cr/Al
35
36 atomic ratio varying from 0.21 to 2.00 were prepared from pure Fe (99.98wt.%,
37
38 Alfa Aesar), pure Cr (99.999wt.%, Alfa Aesar) and pure Al (99.999wt.%, Alfa
39
40 Aesar) using an inductive furnace. The alloys were cast into rods with a diameter
41
42 of 10 mm and length of 100 mm. The precise composition of the Fe-Cr-Al alloys
43
44 was analyzed, applying (i) inductive coupled plasma-optic emission spectroscopy
45
46 (ICP-OES) to determine the content of the alloying elements Cr and Al, (ii) a
47
48 combustion method to determine the light elements C and S and (iii) hot-
49
50 extraction to determine the light elements O and N. The thus determined chemical
51
52 compositions of the alloys are shown in Table 1.
53
54
55
56
57
58
59

60 The cast rods were cold-rolled to foils with a thickness about 0.2 mm in
several steps and were cut into rectangular specimens ($16 \times 16 \text{ mm}^2$). After being

1
2
3 polished, the foils were encapsulated in a quartz tube with an argon atmosphere
4
5 and annealed at 700°C for 2h followed by air-cooling to obtain a recrystallized
6
7 grain structure (grain size of about 20 - 50 μm). Before nitriding the specimens
8
9 were ground and polished (last step: 1 μm diamond paste) and then cleaned in
10
11 ethanol with ultrasonic agitation.
12
13

14 15 16 17 2.2 Nitriding; determination of nitrogen-absorption isotherms

18
19 The foils were suspended at a quartz fiber and placed in the middle of a vertical
20
21 quartz tube furnace. The composition of the ammonia/hydrogen gas mixture
22
23 (purity: NH₃ > 99.998 vol.% and H₂ > 99.999 vol.%) within the furnace was
24
25 precisely controlled by fixing the ratio of the gas flows of both gases, using mass
26
27 flow controllers. A linear gas velocity of 13.5 mm/s (at room temperature) was
28
29 established by keeping the gas flow rate at 500 ml/min in view of the inner
30
31 diameter of 28 mm of the quartz tube furnace. This linear gas flow is sufficient to
32
33 avoid any significant (thermal) decomposition of ammonia in the nitriding
34
35 atmosphere (cf. section 1 and Ref. 9).
36
37
38
39

40
41 In order to maintain a homogeneous precipitation morphology within the
42
43 entire specimen during the determination of the nitrogen-absorption isotherms,
44
45 pre- and de-nitriding experiments were carried out prior to the absorption-
46
47 isotherm experiments. The pre-nitriding was performed at 580°C for 48h with a
48
49 nitriding potential of $r_N (\equiv \frac{P_{NH_3}}{P_{H_2}^{3/2}}$, with p_i as partial pressure of component i [8])
50
51 = 0.104 atm^{-1/2}. This treatment ensures through nitriding of the specimen, without
52
53 iron-nitride formation at the surfaces of the specimen. The specimen was
54
55 quenched into water at room temperature after the pre-nitriding, and subsequently
56
57
58
59
60

1
2
3 de-nitrided in a H₂ atmosphere at 470°C for 72h. By de-nitriding part of the
4
5 nitrogen taken up by the specimen was removed (for this, see section 3.4).
6
7

8 Nitrogen-absorption isotherms were then determined at a temperature of
9
10 560°C. At this temperature (below the pre-nitriding temperature), the precipitation
11
12 morphology of the samples does not change. The determination of the absorption
13
14 isotherms was performed by determining the nitrogen uptake of foils after
15
16 nitriding at 560°C for 72h at each of the following nitriding potentials: $r_N = 0.140$,
17
18 0.117, 0.091 and 0.054 atm^{-1/2} (under these nitriding conditions no iron nitrides
19
20 can be formed at the surfaces of the specimen). The nitriding and de-nitriding
21
22 conditions for the different alloys have been gathered in Table 2.
23
24
25
26

27 The amount of nitrogen taken up was determined by weight measurements
28
29 before and after nitriding using a Mettler microbalance with an accuracy of 0.1
30
31 µg. In order to obtain an accurate weight, the average value of ten measurements
32
33 was taken. The error bars and ranges indicated in Figs. 2b, 5-7 and Tables 3-7,
34
35 respectively, represent the maximal deviation from the average value calculated
36
37 on the basis of the ten weight measurements.
38
39
40
41
42

43 2.3 X-ray diffraction

44 X-ray diffractograms were recorded from the surface of all specimens before and
45
46 after nitriding using a PANalytical (formerly Philips) X'Pert Multi-Purpose
47
48 Diffractometer (MPD) in Bragg-Brentano geometry equipped with a graphite-
49
50 diffracted beam monochromator set to Co-K_α ($\lambda=1.7889\text{Å}$) radiation. The
51
52 specimens were rotated on a spinner around their vertical axis during each
53
54 measurement, to improve crystal statistics. The diffraction angle 2θ was scanned
55
56 over a range from 40° until 120° in steps of 0.05°. Detected phases were identified
57
58 by the 2θ positions of their diffraction peaks in comparison with data from the
59
60

1
2
3 ICDD data base [39]. The diffractograms were evaluated by fitting a Pearson VII
4
5 profile-shape function, using Profile Fit 1.0c software, for the determination of
6
7 peak position and full width at half maximum (FWHM) in the diffractograms.
8
9

10 11 12 2.4 Transmission electron microscopy and electron energy loss spectroscopy

13
14 Specimens for transmission electron microscopy (TEM) were prepared from the
15
16 middle of the specimen as follows.
17
18

19
20 Discs ($\Phi = 3$ mm) were punched out from sheets produced by removing
21
22 material mechanically from both sides (faces) of a nitrided specimen. These discs
23
24 were thinned by applying jet-electropolishing technique using a Struers Tenupol-3
25
26 apparatus (bath composition: 85vol.% acetic acid and 15vol.% perchloric acid,
27
28 current: $26 \text{ mA} \leq I \leq 41 \text{ mA}$, voltage: $15\text{V} \leq U \leq 20.5\text{V}$, temperature: $278\text{K} \leq T \leq$
29
30 280K , flow rate setting “20” at a Struers Tenupol-3 apparatus and treatment time
31
32 $160\text{s} \leq t \leq 275\text{s}$). After jet-electropolishing, the specimens were subsequently
33
34 rinsed in ethanol, acetone and isopropanol. To generate a hole in the middle of the
35
36 sample, the discs were fixed during the jet-electropolishing treatment between two
37
38 platinum rings.
39
40
41
42

43
44 TEM analysis was performed using a Philips CM 200 transmission
45
46 electron microscope operating at 200 kV. Bright field (BF) images and selected
47
48 area diffraction patterns (SADPs) were taken by a CCD camera attached to the
49
50 TEM apparatus.
51
52

53
54 Electron energy loss spectroscopy (EELS) was performed in a Zeiss 912
55
56 Omega TEM operating at 120 kV equipped with an in-column omega-type
57
58 electron spectrometer. For the elemental mappings the “three-window method”
59
60 was used: Two pre-edge images are recorded, which enables the background to be
fitted according to an inverse power law ($I = AE^{-r}$, where I is the intensity, E is the

1
2
3 energy loss and A and r are two fitting parameters) at each pixel in the image. The
4
5 extrapolated background image is then subtracted from the post-edge image (i.e.
6
7 at the ionization edge of the element of interest) to get the elemental map of
8
9 interest which is weak as compared to the background contribution [40].
10
11
12
13
14

15 2.5 Electron probe microanalysis

16
17 The homogeneity of the distribution of the alloying elements Cr and Al and of
18
19 nitrogen in the specimens was confirmed by electron probe microanalysis
20
21 (EPMA) using a Cameca SX100 instrument. Pieces of the specimen were cut to
22
23 prepare cross-sections by subsequently embedding of these pieces with Polyfast
24
25 (Struers; a conductive bakelite resin with carbon filler embedding material),
26
27 followed by grinding and polishing (last step: 1 μm diamond paste). A focused
28
29 electron beam at an accelerating voltage of 15 kV and a current of 100 nA was
30
31 applied. The concentrations of Fe, Cr, Al and N in the specimen were determined
32
33 by measuring the intensities of the characteristic Fe- K_{β} , Cr- K_{α} , Al- K_{α} and N- K_{α}
34
35 X-ray emission peaks at points 2 μm apart along lines traversing the entire
36
37 specimen cross-sections. The concentration of each element was obtained by
38
39 applying the $\Phi(\rho z)$ -correction to the ratio of characteristic X-ray emission peak
40
41 intensities of the specimen and that of a standard specimen (i.e. pure Fe, pure Cr,
42
43 pure Al and γ' -Fe₄N). [41].
44
45
46
47
48
49
50
51
52

53 3. Results and evaluation

54 3.1 Pre-nitriding

55
56 To maintain a homogeneous precipitation morphology in the diffusion zone of the
57
58 specimen during the nitrogen-absorption isotherm measurements a pre-nitriding
59
60 treatment has been applied at an elevated temperature, i.e. a temperature higher

1
2
3 than that applied for nitrogen-absorption isotherm determination. Further the (pre-
4
5)nitriding time should be long enough to establish homogeneity by through
6
7 nitriding of the specimen. Thus the pre-nitriding treatment was performed for each
8
9 alloy specimen (i.e. Cr/Al = 0.21, 0.52, 1.04 and 2.00) at 580°C for 48h with $r_N =$
10
11 0.104 atm^{-1/2}.
12
13

14
15 X-ray diffractograms recorded before and after pre-nitriding of Fe-Cr-Al
16
17 (Cr/Al = 2.00) alloy are shown in Fig. 1a. Only α -Fe reflections can be observed
18
19 before and after pre-nitriding. However, pronounced broadening of the α -Fe
20
21 reflections after pre-nitriding occurs. The absence of separate nitride reflections
22
23 and the strong broadening of the ferrite reflections are indicative of development
24
25 of fine and coherent inner nitride precipitates within the ferrite matrix: the nitrides
26
27 diffract coherently with the surrounding matrix (cf. the extensive discussion for
28
29 nitrided Fe-V alloys in Ref. 42). The diffraction-line broadening is relatively most
30
31 pronounced for the $200_{\alpha\text{-Fe}}$ reflection which is caused by the anisotropic nature of
32
33 the (tetragonal) misfit-strain field around the nitride precipitate and the
34
35 consequence of a Bain-type orientation relationship [42, 43] between the $\text{Cr}_1\text{-}$
36
37 xAl_xN nitride precipitates and the ferrite matrix [38]. The diffraction-line
38
39 broadening (as represented by the full width at half maximum, FWHM) increases
40
41 with increasing Cr/Al ratio (Figs. 1b and c). In addition to the diffraction-line
42
43 broadening, a shift of the intensity maximum of the $200_{\alpha\text{-Fe}}$ reflection towards
44
45 lower diffraction angle, 2θ , occurs upon nitriding. This shift of the $200_{\alpha\text{-Fe}}$
46
47 intensity maximum also increases with increasing Cr/Al ratio (Figs. 1b and c).
48
49
50
51
52
53

54
55 The EPMA elemental-concentration depth profiles presented in Fig. 2a
56
57 show that the concentrations of both alloying elements and of nitrogen are
58
59 constant over the cross section of the specimen; distinct segregation at grain
60
boundaries was not observed. For all (pre-) nitrided alloys/specimens the total

1
2
3 amount of nitrogen, $[N]_{tot}$, taken up after pre-nitriding, as determined by EPMA
4 measurements, matches within experimental accuracy the value as obtained by
5 weight-change measurement.
6
7
8
9

10 Evidently, after the homogeneous nitriding, the nitrogen uptake is larger
11 than the amount of nitrogen required for the precipitation of all alloying element
12 as nitride, $[N]_{(Me_1, Me_2)N}$, plus the amount of nitrogen necessary to establish the
13 equilibrium solubility in an unstrained ferrite matrix, $[N]_{\alpha}^0$. This so called
14 amount of “normal” nitrogen, $[N]_{nor} \equiv [N]_{(Me_1, Me_2)N} + [N]_{\alpha}^0$, has been indicated
15 by the horizontal, dashed line in Fig. 2a. The difference between the
16 experimentally obtained total amount of nitrogen, $[N]_{tot}$, and the amount of
17 “normal” nitrogen, $[N]_{nor}$, is defined as excess nitrogen, $[N]_{ex}$. Comparing the
18 amounts of nitrogen taken up by the various alloys, it follows that the value of
19 $[N]_{tot}$, and thus the value of $[N]_{ex}$, after pre-nitriding increases with decreasing
20 Cr/Al ratio (Fig. 2b).
21
22
23
24
25
26
27
28
29
30
31
32
33
34
35
36
37
38
39
40
41

42 3.2 De-nitriding

43 Subsequent to the pre-nitriding, and also after the determination of each nitrogen-
44 absorption isotherm, each alloy specimen was de-nitrided at 470°C in pure H₂
45 (500 ml/min) for 72h (see section 2.2). For each alloy, the remaining amounts of
46 nitrogen after de-nitriding in both cases (after pre-nitriding and after nitrogen-
47 absorption isotherm determination) are the same. This demonstrates that no
48 significant aging effects (i.e. agglomeration and/or coarsening of nitride
49 precipitates) occurred during the nitrogen-absorption isotherm measurements.
50
51
52
53
54
55
56
57
58
59
60

3.3 Morphology and crystallography of nitride precipitates

1
2
3 TEM bright field (BF) images obtained from pre-nitrided Fe-Cr-Al (Cr/Al = 2.00,
4 1.04 and 0.52) alloys showed that the nitrides precipitate as fine platelets
5 surrounded by distinct strain-field contrast caused by the elastic distortion of the
6 matrix around the misfitting precipitates (see Figs. 3a-c). From the micrographs it
7 follows that the length of the nitride platelets increases (and the platelet density
8 decreases) with decreasing Cr/Al atomic ratio.
9

10
11 Selected area diffraction patterns (SADPs) recorded from all specimens
12 show diffraction spots at locations corresponding to the ferrite matrix. Further,
13 streaks through the 200 and 020 type diffraction spots of the ferrite matrix can be
14 observed. Intensity maxima on these streaks occur (see upper-right insets of Figs.
15 3a-c), at positions expected for 002 type spots of a cubic, rock-salt crystal-
16 structure type nitride precipitate (see what follows).
17

18
19 The SADPs, with their streaks and diffraction spots, are compatible with
20 the presence of nitride precipitates of cubic, rock-salt crystal-structure type in the
21 ferrite matrix (bcc) satisfying a Bain orientation relationship:
22
23
24
25
26
27
28
29
30
31

$$(001)_{\alpha\text{-Fe}} // (001)_{\text{MeN}}, [100]_{\alpha\text{-Fe}} // [110]_{\text{MeN}} : \text{Me} = \text{Cr, Al}$$

32
33
34
35
36
37
38
39
40
41
42
43
44
45
46 The composition of the nitride platelets was investigated by electron
47 energy loss spectroscopy (EELS). Comparing a TEM BF image comprising a part
48 of the ferrite matrix containing precipitate platelets with correspondingly recorded
49 elemental maps for N, Cr and Al (using N-K, Cr-L_{2,3} (+ O-K) and Al-L_{2,3}-
50 ionization edges) shows that N, Cr and Al enrichment occurs at the same
51 locations, there where the precipitate platelets are observed in the TEM BF image
52 (see arrows in Figs. 4a-d). Evidently the nitride precipitates developed as a mixed
53 nitride: Cr_{1-x}Al_xN.
54
55
56
57
58
59
60

1
2
3
4
5
6
7
8
9
10
11
12
13
14
15
16
17
18
19
20
21
22
23
24
25
26
27
28
29
30
31
32
33
34
35
36
37
38
39
40
41
42
43
44
45
46
47
48
49
50
51
52
53
54
55
56
57
58
59
60

Streaks through the 200 and 020 type spots of the ferrite matrix occur in particular for high Cr/Al atomic ratio; in that case the intensity maxima at the 002 type nitride spot positions on the streaks are less pronounced or even absent (cf. Fig. 3a). The reverse holds for low Cr/Al atomic ratio: less pronounced streaks and clearer intensity maxima (cf. Fig. 3c). Streaks, through 200 and 020 type ferrite-matrix diffraction spots, instead of separate nitride diffraction spots, are indicative of a highly coherent nature of the nitride/matrix interface and anisotropic misfit-strain in the ferrite matrix (in particular perpendicular to (001) ferrite-matrix lattice planes) due to the ultra-fine nitride precipitates, which can diffract coherently with the matrix (cf. Fig. 1 and its discussion in section 3.1). The decrease of the extent of streaking with decreasing Cr/Al atomic ratio in the specimen, indicates that the degree of coherency of the nitride precipitates with the ferrite matrix decreases, which development culminates with the emergence of 002 type diffraction spots of nitride precipitates of cubic, rock-salt crystal-structure type (Fig. 3c). Hence, the degree of coherency at the nitride-platelet/matrix interface increases with increasing Cr/Al atomic ratio.

3.4 Nitrogen-absorption isotherms

A nitrogen-absorption isotherm shows the dependence of the amount of nitrogen taken up by a (homogeneously) nitrated specimen as function of the nitrating potential, r_N (directly related to the chemical potential of nitrogen absorbed in the ferrite matrix at the ferrite/gas interface as imposed by a given nitrating atmosphere [8]). The analysis of nitrogen-absorption isotherms allows distinction of the various kinds of differently (chemically) bonded nitrogen in the specimen.

The amount of nitrogen dissolved in the ferrite matrix upon nitrating by means of an NH_3/H_2 gas mixture can be described by the equilibrium:



where $[N]_{\alpha}$ denotes the amount of interstitially dissolved nitrogen in the octahedral interstices of the ferrite matrix. If K denotes the equilibrium constant of the above reaction it is immediately obtained for the concentration of dissolved nitrogen, $[N]_{\alpha}$

$$[N]_{\alpha} = K \cdot r_N \quad (2)$$

In view of the relatively small amount of dissolved nitrogen, Henrian behavior can be assumed and thus the equilibrium constant, K , is supposed to incorporate the constant activity coefficient of dissolved nitrogen and thus is adopted as an effective equilibrium constant.

The nitrogen-absorption isotherms, as recorded after subsequent pre- and de-nitriding treatments (see sections 3.1 and 3.2), are shown for Fe-Cr-Al, with Cr/Al = 0.21, 0.52, 1.04 and 2.00, in Figs. 5a-d, respectively (see also Table 3).

At constant temperature the amount of interstitially dissolved nitrogen in the ferrite matrix should depend linearly on the nitriding potential, r_N (cf. Eq. (2)). Indeed, a straight line can be fitted well (using the least-squares method) to the data points of the total nitrogen content as function of the nitriding potential (dashed lines in Figs. 5). The extrapolation of such straight lines to nitriding potential $r_N = 0$ yields the nitrogen level indicated with 'C' on the ordinates as shown in Figs. 5a-d. The total nitrogen content minus nitrogen level C represents the nitrogen dissolved interstitially in the ferrite matrix.

The amounts of dissolved nitrogen are considerably larger than the amounts expected for pure ferrite in unstrained state (indicated with $[N]_{\alpha}^0$ in

1
2
3 Figs. 5a-d, using literature data for pure ferrite [33]). The dissolved nitrogen in
4
5 excess of $[N]_{\alpha}^0$ is ascribed to the effect of a hydrostatic tensile stress component
6
7 induced in the matrix by elastic accommodation of the misfit between nitride
8
9 precipitate and surrounding matrix (see further below). This type of excess
10
11 nitrogen is denoted as $[N]_{strain}$.
12
13

14
15
16 The nitrogen level 'B' on the ordinates in Figs. 5a-d represents the amount
17
18 of nitrogen left in the specimen after de-nitriding. The nitrogen level indicated
19
20 with 'A' on the ordinates in Figs. 5a-d represents the amount of nitrogen required
21
22 for the formation of the stoichiometric, mixed $Cr_{1-x}Al_xN$ nitride precipitates (i.e.
23
24 $[N]_{Cr_{1-x}Al_xN}$), according to the contents of alloying elements in the specimen (cf.
25
26 Table 1). Values for the nitrogen levels A, B and C for the specimens of different
27
28 Cr/Al atomic ratio have been gathered in Table 4.
29
30
31

32
33 The difference between the nitrogen levels C and A is interpreted as
34
35 nitrogen taken up (hypothetically at $r_N = 0$) in excess of the amount of nitrogen
36
37 necessary to precipitate all Cr and Al as $Cr_{1-x}Al_xN$. It has been proposed that this
38
39 excess nitrogen is located in *adsorbed* fashion at the faces of the (highly coherent)
40
41 nitride platelets (in octahedral interstices on top of Me atoms in the nitride-platelet
42
43 surface; see also Ref. 33). Therefore the type of excess nitrogen represented by
44
45 the difference $C - A$ is denoted as $[N]_{interface}$. The values determined for
46
47 $[N]_{interface}$ have been gathered in Table 5. Evidently, $[N]_{interface}$ pronouncedly
48
49 increases with decreasing Cr/Al atomic ratio.
50
51
52
53

54
55 The composition of a $Cr_{1-x}Al_xN$ precipitate, incorporating the interfacial
56
57 adsorbed excess nitrogen, $[N]_{interface}$, can be described as $Cr_{1-x}Al_xN_y$, where
58
59
60

$$y = \frac{[N]_{Cr_{1-x}Al_xN} + [N]_{interface}}{[N]_{Cr_{1-x}Al_xN}} = \frac{level\ C}{level\ A} \quad (3)$$

The value of y thus obtained contains indirect information on the average thickness of the precipitate platelet. As shown above (see section 3.3), $Cr_{1-x}Al_xN$ precipitates develop as platelets of cubic, rock-salt crystal-structure type obeying a Bain orientation relationship with the ferrite matrix. With $\{001\}_{Cr_{1-x}Al_xN}$ as habit plane, the thickness of a monolayer of $Cr_{1-x}Al_xN$ is one half of the lattice parameter of the rock-salt crystal structure (i.e. $\frac{a_{Cr_{1-x}Al_xN}}{2}$). If at every octahedral interstice in the ferrite matrix at the nitride/matrix interface one excess nitrogen atom is trapped (i.e. on top of a Me atom), it follows

$$y = \frac{n+2}{n} \quad (4)$$

where n is the number of $Cr_{1-x}Al_xN$ monolayers comprising the platelet. Thus the thickness t of a $Cr_{1-x}Al_xN$ platelet follows from

$$t = n \cdot \frac{a_{Cr_{1-x}Al_xN}}{2} = \frac{a_{Cr_{1-x}Al_xN}}{y-1} \quad (5)$$

The lattice parameter of mixed $Cr_{1-x}Al_xN$ nitride can be calculated, for the Cr/Al atomic ratio concerned, by assuming that the lattice constant of mixed $Cr_{1-x}Al_xN$ nitride complies with Vegard's law and taking the lattice parameters of CrN (rock-salt crystal structure) and AlN (rock-salt crystal structure) as 4.14\AA [44] and 3.94\AA [45], respectively. Then the nitride-platelet thicknesses can be calculated using Eq. (5) from the now known values of y (cf. Eq. (3)) and $a_{Cr_{1-x}Al_xN}$. The

results are presented in Table 6. It follows that the thickness of the nitride platelets increases with increasing Cr/Al atomic ratio.

The values obtained for $[N]_{strain} (= [N]_{tot} - [N]_{\alpha}^0 - C)$ are shown as function of nitriding potential, r_N , in Fig. 7. Clearly, at constant r_N , $[N]_{strain}$ increases with increasing Cr/Al atomic ratio.

The presence of misfitting second phase particles in a matrix can lead to elastic distortions of the surrounding matrix. The corresponding stress field (characterized by a tensile hydrostatic component [46, 47]) influences the thermodynamics of nitrogen dissolution in the ferrite matrix. The enhancement of the lattice solubility, i.e. $[N]_{strain}$, with respect to that of the reference state (i.e. $[N]_{\alpha}^0$ for unstrained ferrite) can be given by [48]:

$$\frac{[N]_{\alpha}}{[N]_{\alpha}^0} = \exp \left[\frac{V_N}{RT} \left(\frac{4\varepsilon G_{\alpha}}{(1+\varepsilon)^3} C Y_{(Me_1, Me_2)N_y}^0 \right) \right] \quad (6)$$

where $[N]_{\alpha} = [N]_{\alpha}^0 + [N]_{strain}$ and with

$$\text{misfit parameter: } \varepsilon = \frac{[V_{(Me_1, Me_2)N} + (y-1)fV_{(Me_1, Me_2)N}]^{1/3} - V_{\alpha}^{1/3}}{V_{\alpha}^{1/3}} \quad (7)$$

$$\text{constant: } C = \frac{3K_{(Me_1, Me_2)N}}{(3K_{(Me_1, Me_2)N} + 4G_{\alpha})} \quad (8)$$

volume fraction of $(Me_1, Me_2)N_y$:

$$Y_{(Me_1, Me_2)N_y}^0 = \frac{[Me](V_{(Me_1, Me_2)N} + (y-1)fV_{(Me_1, Me_2)N})}{(1-[Me])V_{\alpha} + [Me](V_{(Me_1, Me_2)N} + (y-1)fV_{(Me_1, Me_2)N})} \quad (9)$$

where V_N is the partial molar volume of nitrogen dissolved in the ferrite matrix, V_{α} and $V_{(Me_1, Me_2)N}$ are the molar volumes of ferrite and the $(Me_1, Me_2)N$ precipitates, y is defined by Eq. (3), G_{α} is the shear modulus of the ferrite matrix, $K_{(Me_1, Me_2)N}$ is the bulk modulus of the $(Me_1, Me_2)N$ precipitate and $[Me]$ ($= [\text{Cr} + \text{Al}]/100$) is the

atomic fraction of alloying elements in the specimen. The parameter f describes the extent to which the full misfit due to building out of the lattice of the $(Me_1, Me_2)N$ precipitates by the adsorbed nitrogen atoms, which act as an entity with the particle, is experienced ($0 \leq f \leq 1$). The following values have been adopted for some of the parameters mentioned above (see Refs. 33 and 48):

$V_N = 5.12 \text{ cm}^3/\text{mol}$; $V_\alpha = 7.092 \text{ cm}^3/\text{mol}$; $G_\alpha = 81.6 \text{ GPa}$; $V_{(Me_1, Me_2)N} = 9.44, 9.67, 9.90 \text{ and } 10.12 \text{ cm}^3/\text{mol}$ for Cr/Al atomic ratios of 0.21, 0.52, 1.04 and 2.00, respectively (using the procedure described below Eq. (5)); $K_{(Me_1, Me_2)N} = 285.98, 300.94, 316.43 \text{ and } 330.67 \text{ GPa}$ for Cr/Al atomic ratios of 0.21, 0.52, 1.04 and 2.00, respectively (derived from the bulk modulus data of $K_{CrN} = 361 \text{ GPa}$ [49] and $K_{AlN} = 270 \text{ GPa}$ [45] as linear function of the Cr/Al atomic ratio).

An experimental value for $[N]_\alpha / [N]_\alpha^0$, at a given nitriding temperature, follows from the ratio of the slopes of the linear parts of the nitrogen-absorption isotherms recorded for Fe-Cr-Al and pure α -Fe:

$$\frac{[N]_\alpha}{[N]_\alpha^0} = \frac{(\Delta[N]_\alpha / \Delta r_N)}{(\Delta[N]_\alpha^0 / \Delta r_N)} = \frac{S_{Fe-Cr-Al}}{S_\alpha^0} \quad (10)$$

where $S_{Fe-Cr-Al}$ and S_α^0 denote the slope of the linear part of the absorption isotherms for Fe-Cr-Al alloys and pure α -Fe, respectively (cf. Fig. 5; the absorption-isotherms for pure α -Fe have been drawn as straight lines passing through the points C on the ordinates, using data from Ref. 33).

The values of all constants at the right-hand side of Eq. (6), except f (cf. Eqs. (7) and (9)), are known and thus by comparing Eqs. (6) and (10), values for f can be straightforwardly calculated from $\frac{S_{Fe-Cr-Al}}{S_\alpha^0}$. The thus obtained values for

f , at $r_N = 0.140 \text{ atm}^{-1/2}$, have been presented in Table 7 as function of the Cr/Al

1
2
3 atomic ratio. It follows that the values obtained for f increase with increasing
4
5 Cr/Al atomic ratio.
6
7
8
9

10 **4. General discussion**

11
12 The equilibrium crystal structures of the nitride precipitates occurring in
13 (recrystallized and subsequently) nitrated Fe-Cr and Fe-Al alloys are the cubic,
14 rock-salt structure for CrN [12, 13, 16] and the hexagonal, wurtzite structure for
15 AlN [23-26]; a metastable rock-salt structure is possible for AlN [50, 51]. The
16 formation of the cubic CrN upon nitriding is relatively fast, whereas the formation
17 of the hexagonal AlN, due to the relatively large volume misfit between this
18 nitride and the ferrite matrix, is relatively very slow [24]. At the nitriding
19 temperature, diffusion of Cr and Al is that slow, as compared to diffusion of N,
20 that the Al atoms are “dragged” into the developing cubic, rock-salt type CrN
21 precipitates: Upon nitriding the system accepts the gain of a smaller than maximal
22 amount of energy, released by nitride precipitation, as an intermediate solution:
23 metastable, mixed $\text{Cr}_{1-x}\text{Al}_x\text{N}$ precipitates develop (see Fig. 4). This has been
24 shown recently to occur for a Cr/Al atomic ratio of 0.52 in Ref. 38. On the basis
25 of this discussion it is likely that a more copious nucleation, i.e. a higher nucleus
26 density of the cubic, rock-salt type, mixed $\text{Cr}_{1-x}\text{Al}_x\text{N}$ nitride, occurs for increasing
27 Cr/Al atomic ratio of the alloy. The results obtained in the present work are in
28 agreement with this prediction (cf. section 3.3).
29
30
31
32
33
34
35
36
37
38
39
40
41
42
43
44
45
46
47
48
49
50
51
52

53 The distinct dependence of $(\text{Me}_1, \text{Me}_2)\text{N}$ nucleus density (and nitride-
54 platelet length and thickness) on Me_1/Me_2 atomic ratio, as observed here for
55 nitrated Fe-Cr-Al alloys, has not been observed for nitrated Fe-Cr-Ti alloys,
56 where mixed $\text{Cr}_{1-x}\text{Ti}_x\text{N}$ nitride platelets of rock-salt crystal structure occur as well
57 for a similar range of the Me_1/Me_2 atomic ratio [52]. Indeed, in the latter case both
58
59
60

1
2
3 equilibrium nitrides (CrN and TiN) have the rock-salt crystal structure, suggesting
4
5 that the ease of nucleation of mixed (Me₁,Me₂)N nitrides is less dependent on
6
7 Me₁/Me₂ atomic ratio for Fe-Cr-Ti alloys than for Fe-Cr-Al alloys.
8
9

10 The coherent nature of the interface between nitride platelet and ferrite
11
12 matrix allows adsorption of nitrogen atoms at the octahedral interstices in the ferrite
13
14 matrix *adjacent to* the platelet faces, as in this way bonding to Cr and/or Al in the
15
16 platelet faces is realized, i.e. $[N]_{interface}$. Now consider: (i) The chemical affinity of
17
18 Al for N is much larger than that of Cr for N. Further, (ii) the thickness of the mixed
19
20 Cr_{1-x}Al_xN nitride platelets decreases with increasing relative Al concentration (i.e.
21
22 with decreasing Cr/Al atomic ratio; see Table 6). Both effects (the chemical one (i)
23
24 and the geometrical one (ii)) explain, that for a constant total atomic alloying
25
26 element content (Cr + Al), $[N]_{interface}$ increases with decreasing Cr/Al atomic ratio,
27
28 as observed (Fig. 6).
29
30
31
32
33
34

35 As follows from the position of level B, relative to the positions of levels C
36
37 and A (cf. Figs. 5a-d), part (or all) of $[N]_{interface}$, and (for the atomic ratio Cr/Al >
38
39 1; cf. Fig. 5) a part of $[N]_{Cr_{1-x}Al_xN}$, can be removed (reversibly!) upon denitriding.
40
41 These removable amounts of nitrogen increase relatively (i.e. with respect to
42
43 $[N]_{interface}$) with increasing Cr/Al atomic ratio. This suggests that the larger the
44
45 relative amount of Al, the smaller the relative amount of such removable nitrogen.
46
47 Indeed the chemical affinity of Al for N is much larger than that of Cr for N. Thus N
48
49 adsorbed at the nitride platelet faces can be overall stronger bonded at smaller Cr/Al
50
51 ratios. A similar discussion may be given for the nitrogen incorporated in a
52
53 metastable Cr_{1-x}Al_xN platelet: at high Cr/Al atomic ratio this nitrogen is less strongly
54
55 bonded, may be partly removed by denitriding during which Cr and Al atoms in the
56
57 nitride platelet remain immobile (note the low temperature of denitriding), so that
58
59
60

1
2
3 upon renitriding the nitrogen deficiency of the platelet becomes repaired, as
4
5 observed.
6
7

8
9 A similar effect was not observed upon nitriding Fe-Cr-Ti alloys: Nitriding
10 leads to the development of $\text{Cr}_{1-x}\text{Ti}_x\text{N}$ mixed nitrides of rock-salt crystal structure in
11 a nitrogen saturated ferrite matrix. Upon denitriding all dissolved nitrogen from the
12 ferrite matrix and all nitrogen adsorbed at the nitride-platelet faces is removed. But,
13 in contrast with the $\text{Cr}_{1-x}\text{Al}_x\text{N}$ platelets, no nitrogen is removed from the $\text{Cr}_{1-x}\text{Ti}_x\text{N}$
14 platelets (for Cr/Ti atomic ratio in the range 0.53 to 2.22) [52]. This may be
15 understood as a consequence of the $\text{Cr}_{1-x}\text{Ti}_x\text{N}$ platelets being relatively more stable
16 (i.e. less metastable) than the $\text{Cr}_{1-x}\text{Al}_x\text{N}$ platelets (note that the equilibrium CrN and
17 TiN nitrides both have a rock-salt crystal structure, whereas the equilibrium AlN
18 nitride has a hexagonal, wurtzite crystal structure).
19
20
21
22
23
24
25
26
27
28
29
30
31

32 The presence of dissolved excess nitrogen in the ferrite matrix upon nitriding
33 of Fe-Cr-Al alloys is a consequence of elastic accommodation of the misfit between
34 nitride platelet and ferrite matrix: such elastic accommodation of misfit induces a
35 tensile hydrostatic stress component in the ferrite matrix [53, 46, 47]. As a
36 consequence, as compared to the unstrained state, more nitrogen can be dissolved
37 (on octahedral interstices) in the ferrite matrix; i.e. $[N]_{\text{strain}}$ [48]. Again comparing
38 recent results obtained upon nitriding Fe-Cr-Ti alloys with the present data obtained
39 for Fe-Cr-Al alloys, it strikes that $[N]_{\text{strain}}$ increases with increasing Cr/Me₂ atomic
40 ratio if Me₂ = Al (Fig. 7) and decreases with increasing Cr/Me₂ atomic ratio if Me₂
41 = Ti [52]. This can be understood as a consequence of the dependence of the
42 nitride/matrix misfit on Cr/Me₂ atomic ratio, as follows.
43
44
45
46
47
48
49
50
51
52
53
54
55
56
57
58

59 The parameter ε (cf. Eq. (7)) describes the overall misfit between a “free”,
60 undeformed “inclusion” and an empty, undeformed “cavity” in a matrix. Upon

insertion of the “inclusion” (here: the nitride particle) into the “cavity” in the matrix (here: the ferrite matrix) of finite size a hydrostatic stress is introduced in the matrix (of tensile nature if $\varepsilon > 0$). For the following comparative discussion, the effect of nitrogen adsorbed at the surface of the nitride particle can be ignored and thus ε can be taken as

$$\varepsilon = \left(\frac{V_{(Me_1, Me_2)N}^{1/3} - V_{\alpha}^{1/3}}{V_{\alpha}^{1/3}} \right) \quad (11)$$

Using the values of the lattice parameter of each nitride (4.14Å for rock-salt crystal-structure type CrN [44], 3.94Å for rock-salt crystal-structure type AlN [45] and 4.24Å for rock-salt crystal-structure type TiN [54]) and assuming that the lattice parameters of the mixed $Cr_{1-x}Al_xN$ and $Cr_{1-x}Ti_xN$ nitrides comply with Vegard’s law, ε can be calculated as function of the Cr/Me₂ (Me₂ = Al or Ti) atomic ratio. The results are shown in Fig. 8a. Evidently, ε increases with increasing atomic ratio Cr/Al and decreases with increasing atomic ratio Cr/Ti. It thus is predicted that $[N]_{strain}$ increases with increasing Cr/Al atomic ratio and with decreasing Cr/Ti atomic ratio, as observed (cf. Fig. 7 for Fe-Cr-Al alloys and Ref. 52 for Fe-Cr-Ti alloys).

In view of the observed Bain orientation relationship and the occurring $\{001\}_{\alpha-Fe}$ -type habit plane (cf. section 3.3), the linear misfit along the habit plane (i.e. parallel to the faces of the nitride platelet), $\delta_{//}$ is given by

$$\delta_{//} = \left(\frac{a_{(Me_1, Me_2)N} - a_{\alpha-Fe} \sqrt{2}}{a_{\alpha-Fe} \sqrt{2}} \right) \times 100 \quad (\%) \quad (12a)$$

and the linear misfit perpendicular to this habit plane (i.e. perpendicular to the faces of the nitride platelet), δ_{\perp} , obeys

$$\delta_{\perp} = \left(\frac{a_{(Me_1, Me_2)N} - a_{\alpha-Fe}}{a_{\alpha-Fe}} \right) \times 100 \quad (\%) \quad (12b)$$

Using the same lattice-parameter data as indicated above, $\delta_{//}$ and δ_{\perp} can be calculated as function of the atomic ratio Cr/Me₂. The results are shown in Fig. 8b. For Fe-Cr-Ti alloys both $\delta_{//}$ and δ_{\perp} are positive and decrease with increasing Cr/Ti atomic ratio. For Fe-Cr-Al alloys an antagonistic behaviour occurs: $|\delta_{\perp}|$ increases with increasing Cr/Al atomic ratio, whereas $|\delta_{//}|$ decreases with increasing Cr/Al atomic ratio (for the alloys investigated within the range 0.21-2.00). Although the change of δ_{\perp} dominates the change of the overall misfit parameter ε (cf. Eq. (11) and thus is responsible for the increase of $[N]_{strain}$ with increasing Cr/Al atomic ratio (see above)), the decrease of $|\delta_{//}|$ with increasing Cr/Al atomic ratio suggests that the nitride/matrix coherency at the faces of the nitride platelets increases with increasing Cr/Al atomic ratio and thus explains the observation of the more pronounced streaking through the 200 and 020 type ferrite-matrix diffraction-spots and the disappearing 200 type nitride diffraction spots with increasing Cr/Al atomic ratio (Fig. 3; section 3.3).

The value of f describes the extent to which the volume misfit due to the nitrogen, adsorbed at the interface is experienced (cf. section 3.3). Obviously, given a constant microstructure during the nitrogen absorption-isotherm measurements, the values of f determined in this work as function of the Cr/Al atomic ratio are characteristic for the pre-nitriding temperature (here 580°C). Of course, f will not depend in a direct way on the value of $[N]_{interface}$ (note that with increasing Cr/Al

1
2
3 atomic ratio f increases (cf. Table 7) and $[N]_{interface}$ decreases (cf. Table 5)).
4
5
6 Evidently, f will depend on the degree of coherency at the nitride-platelet/matrix
7
8 interface and thus the increase of f with increasing Cr/Al atomic ratio can be
9
10 conceived as a direct consequence of $|\delta_{//}|$ decreasing with increasing Cr/Al atomic
11
12 ratio (cf. the discussion in the previous paragraph).
13
14
15
16
17
18

19 5. Conclusions

20
21 1. Upon nitriding of Fe-Cr-Al alloys, metastable, mixed $Cr_{1-x}Al_xN$ nitrides of
22
23 cubic, rock-salt crystal-structure type precipitate in the ferrite matrix; the system
24
25 thus avoids the difficult nucleation of stable AlN (hexagonal, wurtzite structure
26
27 type) precipitates in the ferrite matrix. The ease of mixed nitride nucleation and
28
29 thus the nucleation density increases with increasing Cr/Al atomic ratio. Such an
30
31 effect does not occur for nitrated Fe-Cr-Ti alloys as both equilibrium nitrides,
32
33 CrN and TiN, have the same (rock-salt type) crystal structure as the corresponding
34
35 metastable mixed $Cr_{1-x}Ti_xN$ precipitate.
36
37
38
39
40
41

42 2. The amount of excess nitrogen adsorbed at the faces of the nitride platelets,
43
44 $[N]_{interface}$, increases with decreasing Cr/Me₂ (Me₂ = Al or Ti) atomic ratio
45
46 because the chemical affinity of Me₂ for N is much larger than that of Cr for N
47
48 and because the thickness of the nitride platelets decreases with decreasing
49
50 Cr/Me₂ atomic ratio.
51
52
53

54
55
56 3. The amount of excess nitrogen dissolved in the ferrite matrix, $[N]_{strain}$,
57
58 *increases* with increasing Cr/Me₂ atomic ratio for Me₂ = Al and *decreases* with
59
60 increasing Cr/Me₂ atomic ratio for Me₂ = Ti. These antagonistic behaviours can

1
2
3 be understood as consequences of the overall nitride/matrix misfit increasing with
4
5 increasing Cr/Al atomic ratio and decreasing with increasing Cr/Ti atomic ratio.
6
7

8
9
10 4. The degree of coherency at the $\text{Cr}_{1-x}\text{Al}_x\text{N}$ -platelet faces increases with
11
12 increasing Cr/Al atomic ratio (TEM analysis), which reflects the decrease of the
13
14 absolute value of the linear misfit parameter parallel to the interface, $|\delta_{//}|$, with
15
16 increasing Cr/Al atomic ratio (for the alloys investigated within the range 0.21-
17
18 2.00), opposite to the trend for the overall misfit parameter, ϵ .
19
20
21
22
23
24
25
26
27
28
29
30
31
32
33
34
35
36
37
38
39
40
41
42
43
44
45
46
47
48
49
50
51
52
53
54
55
56
57
58
59
60

Acknowledgements

The authors thank Mr. S. Meka M. Tech. for discussion, Dipl. Ing. P. Kress and Mr. J. Koehler for assistance with the nitriding experiments, Mrs. S. Haug for assistance with the EPMA experiments, Mr. W. D. Lang for TEM sample preparation and Dr. W. Sigle for assistance during the EELS experiments and for discussion (all with the Max Planck Institute for Metals Research).

For Peer Review Only

References

- [1] S. Lampman, Introduction to surface hardening of steel ASM Handbook, vol. 4, Heat Treating, ASM International, Metals Park, Ohio, 1991.
- [2] H. Ferkel, M. Glatzer, Y. Estrin, R.Z. Valiev, C. Blawert and B.L. Mordike, Mat. Sci. Eng. A 348 (2003) p.100.
- [3] M. Pellizzari, A. Molinari and G. Straffelini, Mat. Sci. Eng. A 352 (2003) p.186.
- [4] N. Limodin and Y. Verreman, Mat. Sci. Eng. A 435-436 (2006) p.460.
- [5] A. Basu, J. Dutta Majumdar, S. Ghosh Chowdhury, P.K. Ajikumar, P. Shankar, A.K. Tyagi, Baldev Raj and I. Manna, Surf. Coat. Technol. 201 (2007) p.6985.
- [6] T. Hirsch, T.G.R. Clarke and A. da Silva Rocha, Surf. Coat. Technol. 201 (2007) p.6380.
- [7] S. Jegou, L. Barrallier and R. Kubler, Acta Mater. 58 (2010) p.2666.
- [8] E.J. Mittemeijer and J.T. Slycke, Surf. Eng. 12 (1996) p.152.
- [9] E.J. Mittemeijer and M.A.J. Somers, Surf. Eng. 13 (1997) p.483.
- [10] G. Miyamoto, A. Yonemoto, Y. Tanaka, T. Furuhashi and T. Maki, Acta Mater. 54 (2006) p.4771.
- [11] G. Miyamoto, A. Yonemoto, Y. Tanaka, T. Maki and T. Furuhashi, ISIJ International 49 (2009) p.1796.
- [12] B. Mortimer, P. Grieveson and K.H. Jack, Scand. J. Metals 1 (1972) p.203.
- [13] K.H. Jack, Proc. Heat Treatment Conf. London 1973, The Metals Society, London (1975) p.39.
- [14] B.J. Lightfoot and D.H. Jack, Proc. Heat Treatment Conf. London 1973, The Metals Society, London (1975) p.59.
- [15] R.E.E. Pulkkinen, Scan. J. Metall. 12 (1983) p.87.

- 1
2
3 [16] P.M. Hekker, H.C.F. Rozendaal and E.J. Mittemeijer, *J. Mater. Sci.* 20
4
5 (1985) p.718.
6
7
8 [17] R.E. Schacherl, P.C.J. Graat and E.J. Mittemeijer, *Z. Metallkd.* 93 (2002)
9
10 p.468.
11
12 [18] R.E. Schacherl, P.C.J. Graat and E.J. Mittemeijer, *Metall. Mater. Trans. A* 35
13
14 (2004) p.3387.
15
16 [19] S.S. Hosmani, R.E. Schacherl and E.J. Mittemeijer, *Mater. Sci. Technol.* 21
17
18 (2005) p.113.
19
20
21 [20] S.S. Hosmani, R.E. Schacherl and E.J. Mittemeijer, *J. Mater. Sci.* 43 (2008)
22
23 p.2618.
24
25 [21] S.S. Hosmani, R.E. Schacherl, L.L. Dobrzyńska and E.J. Mittemeijer, *Phil.*
26
27 *Mag. A* 88 (2008) p.2411.
28
29
30 [22] H.H. Podgurski, R.A. Oriani and F.N. Davis, *Trans. Metall. Soc. AIME* 245
31
32 (1969) p.1603.
33
34 [23] H.H. Podgurski and H.E. Knechtel, *Trans. Metall. Soc. AIME* 245 (1969)
35
36 p.1595.
37
38 [24] M.H. Biglari, C.M. Brakman, W.G. Sloof, E.J. Mittemeijer and S. Van Der
39
40 Zwaag, *Z. Metallkd.* 84 (1993) p.124.
41
42 [25] M.H. Biglari, C.M. Brakman, E.J. Mittemeijer and S. Van Der Zwaag, *Phil.*
43
44 *Mag. A* 72 (1995) p.1281.
45
46 [26] M.H. Biglari, C.M. Brakman, E.J. Mittemeijer and S. Van Der Zwaag, *Phil.*
47
48 *Mag. A* 72 (1995) p.931.
49
50 [27] H.J. Spies, H. Biermann and A. Fischer, *Z. Metallkd.* 96 (2005) p.781.
51
52 [28] W.D. Welch and S.H. Carpenter, *Acta Metall.* 21 (1973) p.1169.
53
54 [29] M. Pope, P. Grieveson and K.H. Jack, *Scand. J. Metall.* 2 (1973) p.29.
55
56 [30] A.D. Krawitz, *Scripta Metall.* 11 (1977) p.117.
57
58
59
60

- 1
2
3 [31] M.M. Yang and A.D. Krawitz, Metall. Trans. A 15 (1984) p.1545.
4
5 [32] S.S. Hosmani, R.E. Schacherl and E.J. Mittemeijer, Acta Mater. 53 (2005)
6
7 p.2069.
8
9 [33] S.S. Hosmani, R.E. Schacherl and E.J. Mittemeijer, Acta Mater. 54 (2006)
10
11 p.2783.
12
13 [34] D.H. Kirkwood, O.E. Atasoy and S.R. Keown, Metals. Sci. 8 (1974) p.49.
14
15 [35] D.H. Jack, Acta Metall. 24 (1976) p.137.
16
17 [36] D.S. Rickerby, S. Henderson, A. Hendry and K.H. Jack, Acta Metall. 34
18
19 (1986) p.1687.
20
21 [37] H.H. Podgurski and F.N. Davis, Acta Metall. 29 (1981) p.1.
22
23 [38] A.R. Clauss, E. Bischoff, R.E. Schacherl and E.J. Mittemeijer, Metall. Mater.
24
25 Trans. A 40 (2009) p.1923.
26
27 [39] JCPDS-International Center for Diffraction Data (2002), PCPDFWIN,
28
29 Version 2.3
30
31 [40] P. Crozier, Ultramicroscopy 58 (1995) p.157.
32
33 [41] J.L. Pouchou and F. Pichoir, Rech. Aerosp. (1984) p.167.
34
35 [42] N.E. Vives Diaz, S.S. Hosmani, R.E. Schacherl and E.J. Mittemeijer, Acta
36
37 Mater. 56 (2008) p.4137.
38
39 [43] E.C. Bain, Trans. AIME 70 (1924) p.25.
40
41 [44] M. Nasr Eddine, E.F. Bertaut and M. Maunaye, Acta Crystallogr. B 33
42
43 (1977) p.2696.
44
45 [45] N.E. Christensen and I. Gorczyca, Phys. Rev. B 47 (1993) p.4307.
46
47 [46] E.J. Mittemeijer, P. Van Mourik and Th. D. De Keijser, Phil. Mag. A 43
48
49 (1981) p.1157.
50
51 [47] E.J. Mittemeijer and A. Van Gent, Scripta Metall. 18 (1984) p.825.
52
53
54
55
56
57
58
59
60

- 1
2
3 [48] M.A.J. Somers, R.M. Lankreijer and E.J. Mittemeijer, *Phil. Mag. A* 59
4
5 (1989) p.353.
6
7
8 [49] F. Rivadulla, M. Banobre-Lopez, C.X. Quintela, A. Pineiro, V. Pardo, D.
9
10 Baldomir, M.A. Lopez-Quintela, J. Rivas, C.A. Ramos, H. Salva, J.S. Zhou and
11
12 J.B. Goodenough, *Nature Mater.* 8 (2009) p.947.
13
14
15 [50] W.T. Lin, L.C. Meng, G.J. Chen, H.S. Liu, *Appl. Phys. Lett.* 66 (1995)
16
17 p.2066.
18
19
20 [51] Z.M. Ren, Y.F. Lu, H.Q. Ni, T.Y.F. Liew, B.A. Cheong, S. Chow, M.L. Ng
21
22 and J.P. Wang, *J. Appl. Phys.* 88 (2000) p.7346.
23
24
25 [52] K.S. Jung, R.E. Schacherl, E. Bischoff and E.J. Mittemeijer, *HTM J. Heat*
26
27 *Treatm. Mat.* 65 (2010) p.237.
28
29
30 [53] J.D. Eshelby, *Solid St. Phys.* 3 (1956) p.79.
31
32 [54] W. Lengauer, S. Binder, K. Aigner, P. Ettmayer, A. Guillou, J. Debuigne and
33
34 G. Groboth, *J. Alloys. Compd.* 217 (1995) p.137.
35
36
37
38
39
40
41
42
43
44
45
46
47
48
49
50
51
52
53
54
55
56
57
58
59
60

Table 1: The amounts of Cr and Al and light element impurities in the alloy specimens before nitriding.

element alloy	Cr	Al	N	O	S	C
	(at.%)		(µg/g)			
Fe-Cr-Al (Cr/Al = 0.21)	0.26 (±0.007)	1.22 (±0.008)	2 ± 1	12 ± 6	12	14
Fe-Cr-Al (Cr/Al = 0.52)	0.51 (±0.005)	0.99 (±0.009)	2 ± 1	12 ± 6	17	15
Fe-Cr-Al (Cr/Al = 1.04)	0.75 (±0.009)	0.72 (±0.006)	3 ± 1	12 ± 6	12	13
Fe-Cr-Al (Cr/Al = 2.00)	1.00 (±0.005)	0.50 (±0.005)	2 ± 1	12 ± 6	14	12

Table 2: Summary of the nitriding parameters for the Fe-Cr-Al alloys.

	temp. (°C)	time (h)	NH ₃ (ml/min)	H ₂ (ml/min)	r _N (atm ^{-1/2})
pre-nitriding	580	48	45	455	0.104
de-nitriding	470	72	.	500	.
absorption isotherms	560	72	58	442	0.140
			50	450	0.117
			40	460	0.091
			25	475	0.054

Table 3: $[N]_{tot}$ for the Fe-Cr-Al alloys (nitrogen-absorption-isotherm measurements at 560°C for 72h).

alloy	r_N (atm ^{-1/2})	0.054	0.091	0.117	0.140
Fe-Cr-Al (Cr/Al = 0.21): $[N]_{tot}$ (at.%)		2.13 (±0.02)	2.27 (±0.03)	2.34 (±0.02)	2.41 (±0.04)
Fe-Cr-Al (Cr/Al = 0.52): $[N]_{tot}$ (at.%)		2.12 (±0.01)	2.23 (±0.01)	2.32 (±0.01)	2.38 (±0.03)
Fe-Cr-Al (Cr/Al = 1.04): $[N]_{tot}$ (at.%)		1.90 (±0.01)	2.03 (±0.03)	2.11 (±0.02)	2.20 (±0.03)
Fe-Cr-Al (Cr/Al = 2.00): $[N]_{tot}$ (at.%)		1.88 (±0.03)	2.02 (±0.02)	2.10 (±0.01)	2.18 (±0.02)

Table 4: Nitrogen levels 'A', 'B' and 'C' (see Fig. 5), for the Fe-Cr-Al alloys.

N content (at.%) alloy	level A	level B	level C
Fe-Cr-Al (Cr/Al = 0.21)	1.46 (± 0.015)	1.78 (± 0.007)	1.99
Fe-Cr-Al (Cr/Al = 0.52)	1.48 (± 0.014)	1.72 (± 0.005)	1.95
Fe-Cr-Al (Cr/Al = 1.04)	1.45 (± 0.015)	1.40 (± 0.006)	1.71
Fe-Cr-Al (Cr/Al = 2.00)	1.48 (± 0.010)	1.37 (± 0.005)	1.67

Table 5: The values of the $[N]_{interface}$ for the Fe-Cr-Al alloys (after prenitriding at 580°C).

alloy	N content (at.%)	$[N]_{interface}$
Fe-Cr-Al (Cr/Al = 0.21)		0.53 (± 0.015)
Fe-Cr-Al (Cr/Al = 0.52)		0.47 (± 0.014)
Fe-Cr-Al (Cr/Al = 1.04)		0.26 (± 0.015)
Fe-Cr-Al (Cr/Al = 2.00)		0.06 (± 0.010)

Table 6: The mixed $\text{Cr}_{1-x}\text{Al}_x\text{N}_y$ nitride platelet thickness and corresponding y values (cf. Eq. (3)) for the Fe-Cr-Al alloys.

alloy	thickness (nm)	y
Fe-Cr-Al (Cr/Al = 0.21)	1.09 (± 0.03)	1.36 (± 0.010)
Fe-Cr-Al (Cr/Al = 0.52)	1.25 (± 0.05)	1.32 (± 0.012)
Fe-Cr-Al (Cr/Al = 1.04)	2.24 (± 0.14)	1.18 (± 0.012)
Fe-Cr-Al (Cr/Al = 2.00)	2.66 (± 0.13)	1.15 (± 0.008)

Table 7: The values for $\frac{S_{Fe-Cr-Al}}{S_{\alpha}^0}$ and f (cf. Eqs. (6-9)) at the nitriding potential, $r_N = 0.140 \text{ atm}^{-1/2}$ for the Fe-Cr-Al alloys.

alloy	$\frac{S_{Fe-Cr-Al}}{S_{\alpha}^0}$	f
Fe-Cr-Al (Cr/Al = 0.21)	1.35 (± 0.009)	0.10 (± 0.04)
Fe-Cr-Al (Cr/Al = 0.52)	1.39 (± 0.012)	0.12 (± 0.01)
Fe-Cr-Al (Cr/Al = 1.04)	1.58 (± 0.009)	0.84 (± 0.04)
Fe-Cr-Al (Cr/Al = 2.00)	1.65 (± 0.009)	0.96 (± 0.04)

Figure captions

Figure 1a X-ray diffractograms ($40^\circ < 2\theta < 120^\circ$; Co- K_α radiation) before and after pre-nitriding of Fe-Cr-Al (Cr/Al = 2.00) alloy (note the logarithmic intensity scale). The nitriding experiment was performed at 580°C for 48h with nitriding potential $r_N = 0.104 \text{ atm}^{-1/2}$.

Figure 1b X-ray diffractograms of the $200_{\alpha\text{-Fe}}$ reflection ($75^\circ < 2\theta < 80^\circ$, normalized with respect to integrated intensity; Co- K_α radiation) after prenitriding of Fe-Cr-Al (Cr/Al = 0.21, 0.52, 1.04 and 2.00) alloys.

Figure 1c The full width at half maximum (FWHM) and the position of the intensity maximum of the $200_{\alpha\text{-Fe}}$ reflection evaluated by fitting a Pearson VII profile-shape function as function of the Cr/Al atomic ratio.

Figure 2a Concentration-depth profiles for N, Cr and Al as determined by EPMA after pre-nitriding (48h at 580°C with $r_N = 0.104 \text{ atm}^{-1/2}$) of the Fe-Cr-Al (Cr/Al = 2.00) specimen. The horizontal line denotes the amount of “normal” nitrogen, $[N]_{nor}$: sum of the amounts of nitrogen necessary to precipitate all alloying elements as alloying element nitrides, $[N]_{Cr-xAl_xN}$, and of nitrogen dissolved interstitially in the unstrained ferrite matrix, $[N]_\alpha^0$.

Figure 2b The total amount of nitrogen taken up by the specimen, $[N]_{total}$, which can be compared with the amount of normal nitrogen, $[N]_{nor}$ (see also Fig. 2a), as function of the Cr/Al atomic ratio (after pre-nitriding of the Fe-Cr-Al alloys).

Figure 3 TEM bright field images (left; electron-beam direction $[001]_{\alpha\text{-Fe}}$) showing platelet-type nitride precipitation in the ferrite matrix. (a) Fe-Cr-Al

1
2
3 (Cr/Al = 2.00), (b) Fe-Cr-Al (Cr/Al = 1.04) and (c) Fe-Cr-Al (Cr/Al = 0.52). The
4
5
6 corresponding SADPs are shown in the insets. Streaks passing through 200 and
7
8 020 type ferrite diffraction spots become less pronounced with decreasing Cr/Al
9
10 atomic ratio and even intensity maxima at the position expected for 002 type
11
12 diffraction spots of cubic, rock-salt crystal-structure type nitride become
13
14 observable for the lowest Cr/Al atomic ratio (further, see text). Schematic
15
16 diffraction patterns (right), corresponding with the SADPs shown, comply with a
17
18 Bain orientation relationship of the nitride platelets with the α -Fe matrix (black
19
20 dots: diffraction spots of the ferrite matrix; open circles: diffraction spots of the
21
22 cubic, rock-salt crystal-structure type nitride precipitates). The spots in the SADPs
23
24 at the position of forbidden $100_{\alpha\text{-Fe}}$ reflections, denoted by “x” in the schematic
25
26 SADPs, are $220_{\text{Fe}_3\text{O}_4}$ spots caused by an iron oxide (Fe_3O_4) layer developed on the
27
28 surface of the foil during TEM sample preparation.
29
30
31
32
33
34
35

36 **Figure 4** (a) TEM bright field image (taken near to the hole in the jet-
37
38 electropolished foil) of the nitrated Fe-Cr-Al (Cr/Al = 0.21) specimen and the
39
40 corresponding elemental maps for (b) N, (c) Cr (+O) and (d) Al, as determined by
41
42 EELS. The arrows indicate the (same) nitride platelet positions in (a)-(d). In case
43
44 of Cr mapping, the background was determined in front of the O-K edge because
45
46 of the overlapping O-K and Cr- L_{2-3} edges. Therefore the Cr mapping contains
47
48 oxygen signal caused by surface oxidation which cannot be avoided.
49
50
51
52
53
54
55
56
57

58 **Figure 5** Nitrogen absorption isotherms for (a) Fe-Cr-Al (Cr/Al = 0.21), (b) Fe-
59
60 Cr-Al (Cr/Al = 0.52), (c) Fe-Cr-Al (Cr/Al = 1.04) and (d) Fe-Cr-Al (Cr/Al = 2.00)
specimens measured at 560°C after subsequent pre- and de-nitrating (cf. section

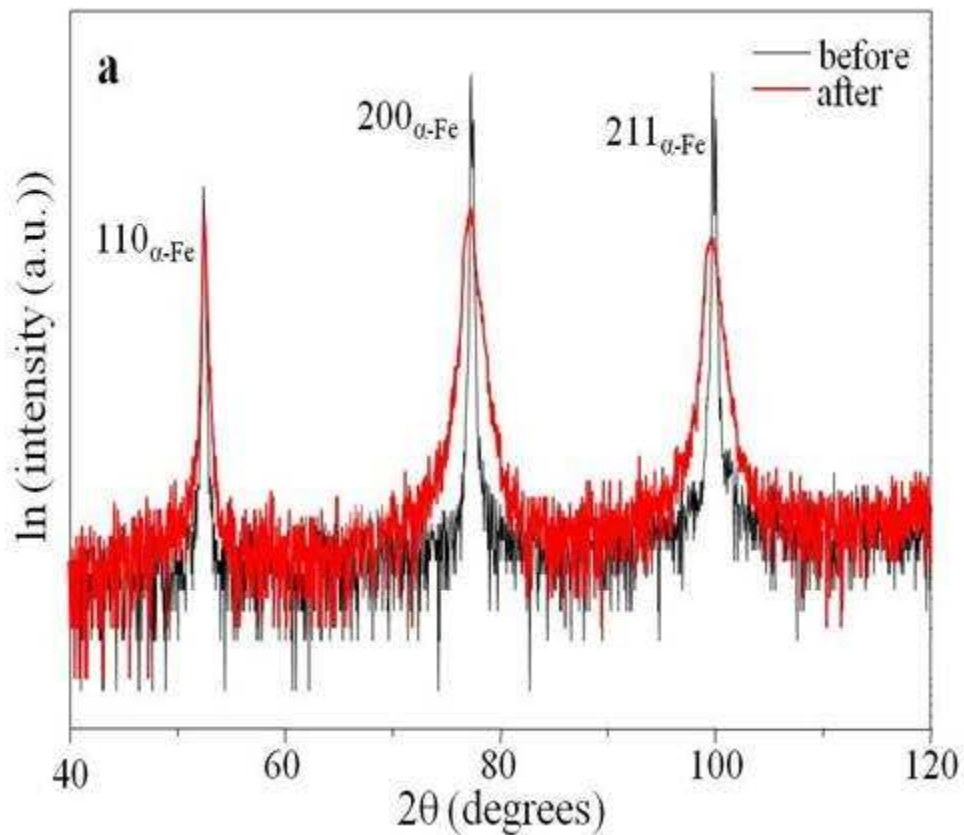
1
2
3 2.2). The level 'A', represents the amount of nitrogen required for complete
4 precipitation of Cr and Al to $\text{Cr}_{1-x}\text{Al}_x\text{N}$; the level 'B' is the amount of nitrogen left
5
6 after de-nitriding and the level 'C' indicates the intersection of the linear portion
7
8 of the absorption isotherm with the ordinate at $r_N = 0$ (further, see text).
9
10
11
12
13
14

15 **Figure 6** $[N]_{\text{interface}}$ as function of the Cr/Al atomic ratio.
16
17
18
19

20 **Figure 7** $[N]_{\text{strain}}$ as function of the Cr/Al atomic ratio. The dashed-lines in the
21
22 figure are least-squares fits of straight lines forced to pass through $r_N = 0$.
23
24
25
26

27 **Figure 8a** The overall misfit, ε (see Eq. (11)), between mixed nitride and ferrite
28
29 matrix as function of Cr/Me₂ (Me₂ = Al or Ti).
30
31
32
33

34 **Figure 8b** The misfit perpendicular (δ_{\perp}) and parallel (δ_{\parallel}) to the $\{001\}_{\alpha\text{-Fe}}$ habit
35
36 plane for mixed $\text{Cr}_{1-x}\text{Al}_x\text{N}$ and $\text{Cr}_{1-x}\text{Ti}_x\text{N}$ nitrides as function of Cr/Me₂ (Me₂ = Al
37
38 or Ti) atomic ratio.
39
40
41
42
43
44
45
46
47
48
49
50
51
52
53
54
55
56
57
58
59
60



35 Fig1a
36 84x70mm (150 x 150 DPI)

1
2
3
4
5
6
7
8
9
10
11
12
13
14
15
16
17
18
19
20
21
22
23
24
25
26
27
28
29
30
31
32
33
34
35
36
37
38
39
40
41
42
43
44
45
46
47
48
49
50
51
52
53
54
55
56
57
58
59
60

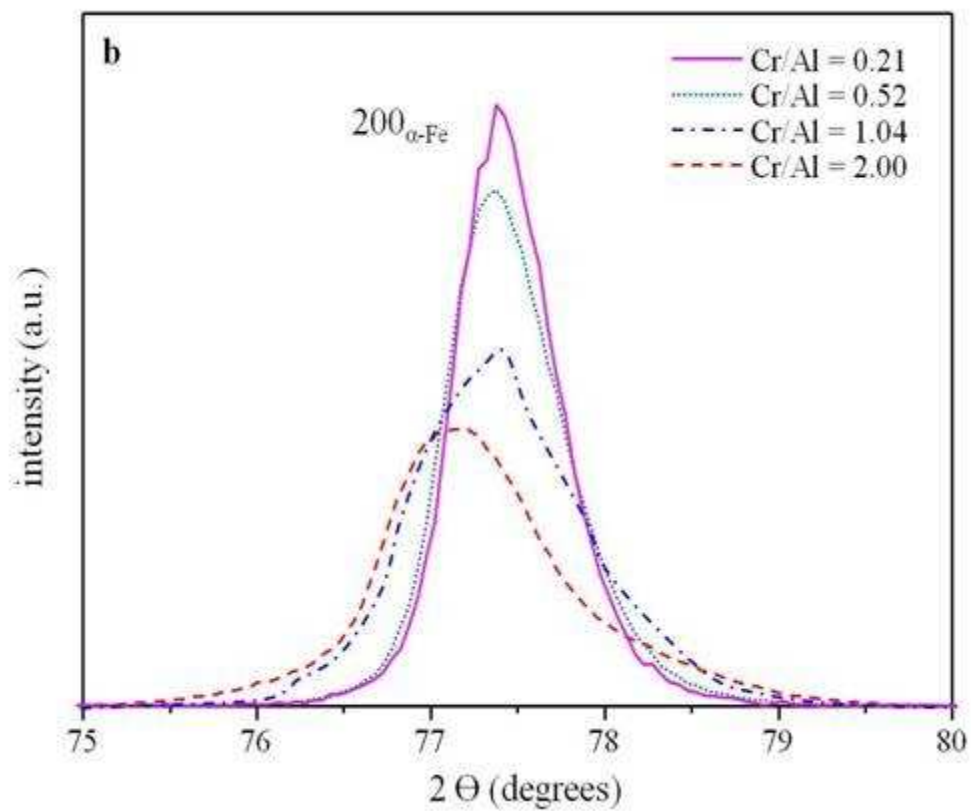


Fig1b
84x70mm (150 x 150 DPI)

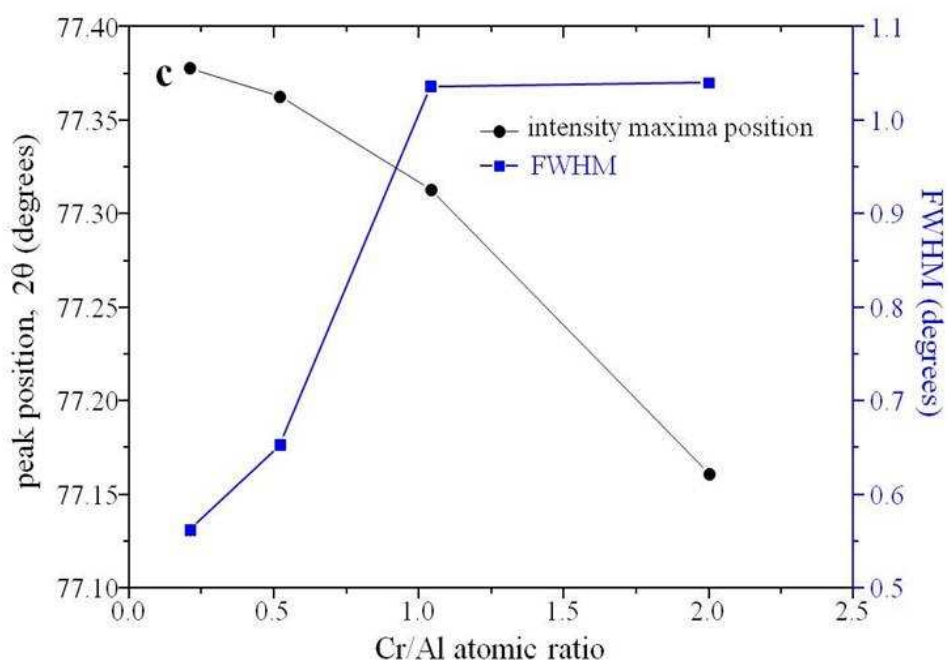


Fig1c
129x90mm (150 x 150 DPI)

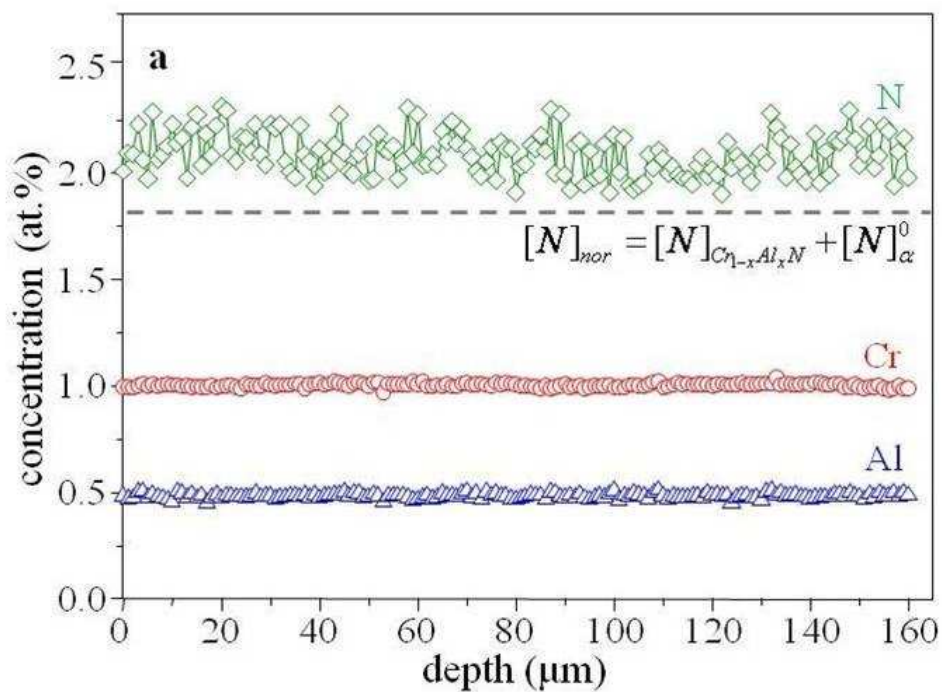


Fig2a
129x90mm (140 x 150 DPI)

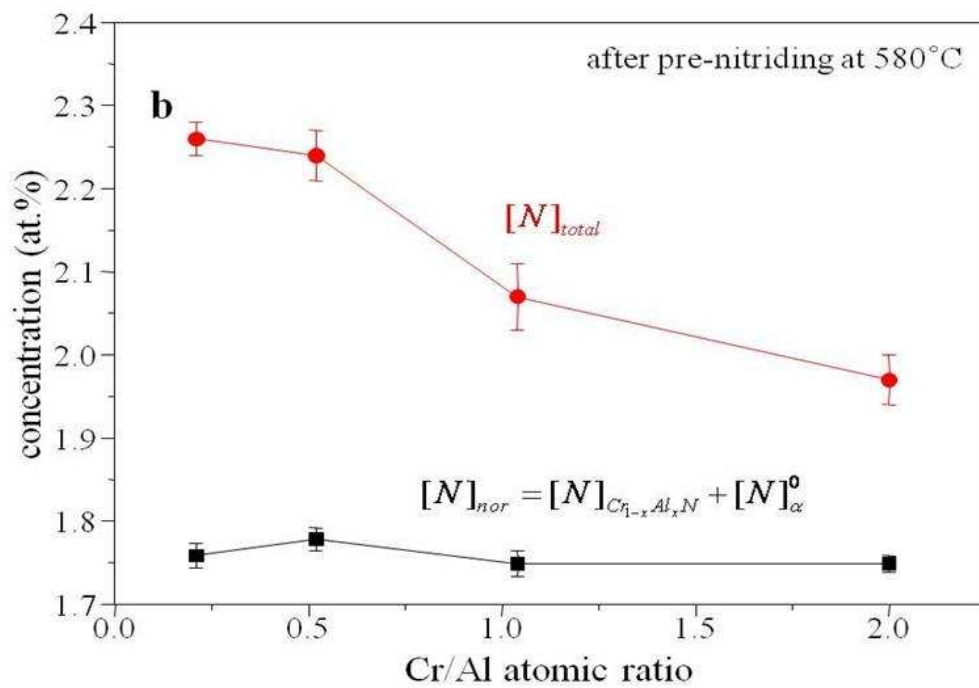


Fig2b
129x90mm (150 x 150 DPI)

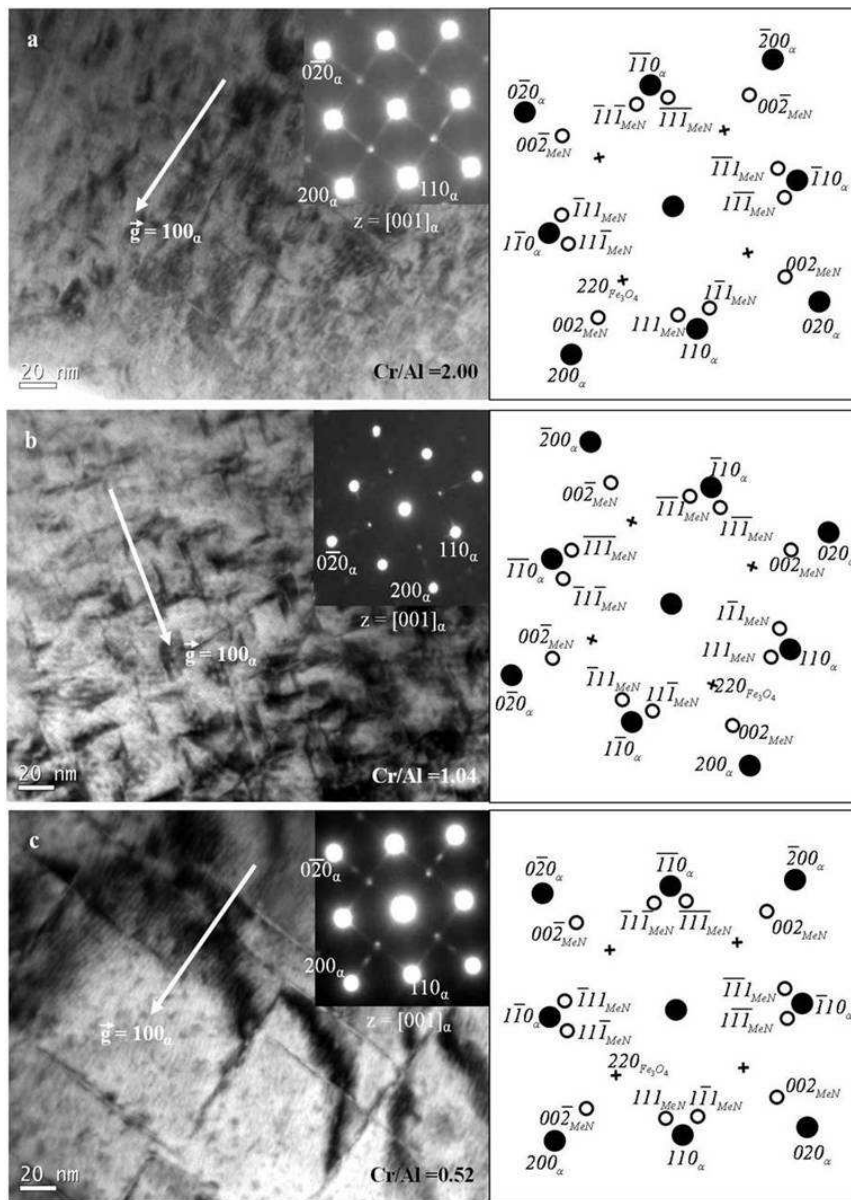


Fig3
129x180mm (150 x 150 DPI)

1
2
3
4
5
6
7
8
9
10
11
12
13
14
15
16
17
18
19
20
21
22
23
24
25
26
27
28
29
30
31
32
33
34
35
36
37
38
39
40
41
42
43
44
45
46
47
48
49
50
51
52
53
54
55
56
57
58
59
60

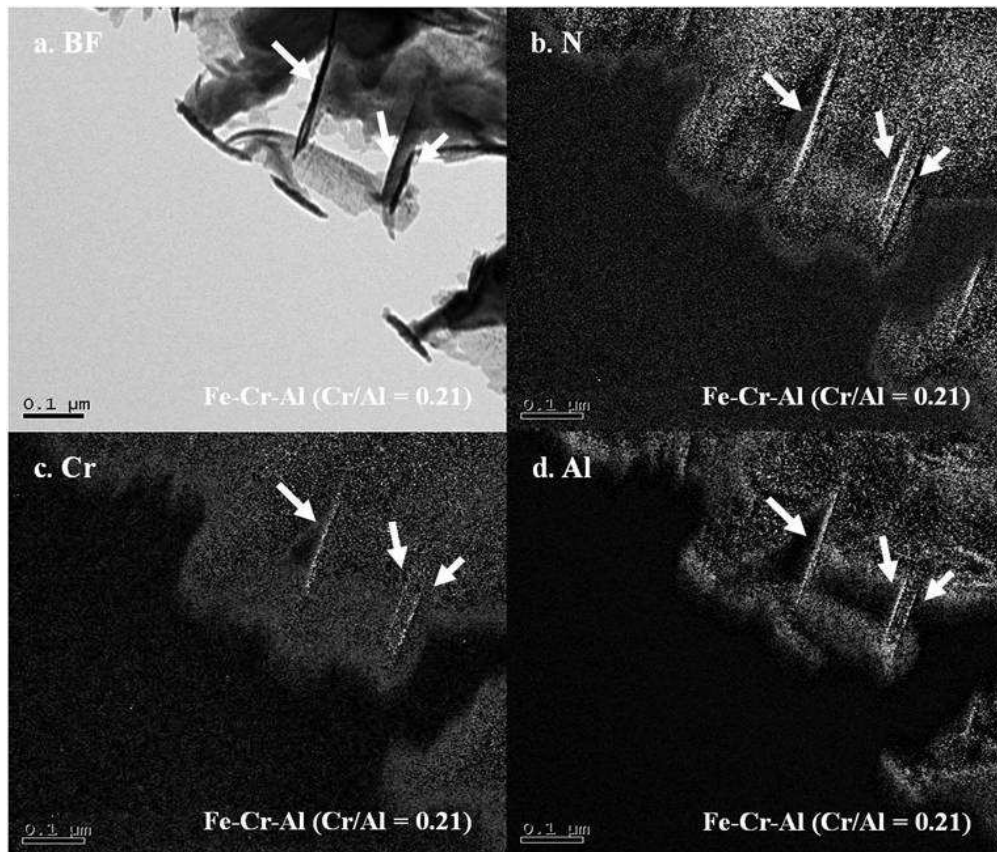


Fig4
129x110mm (150 x 150 DPI)

www Only

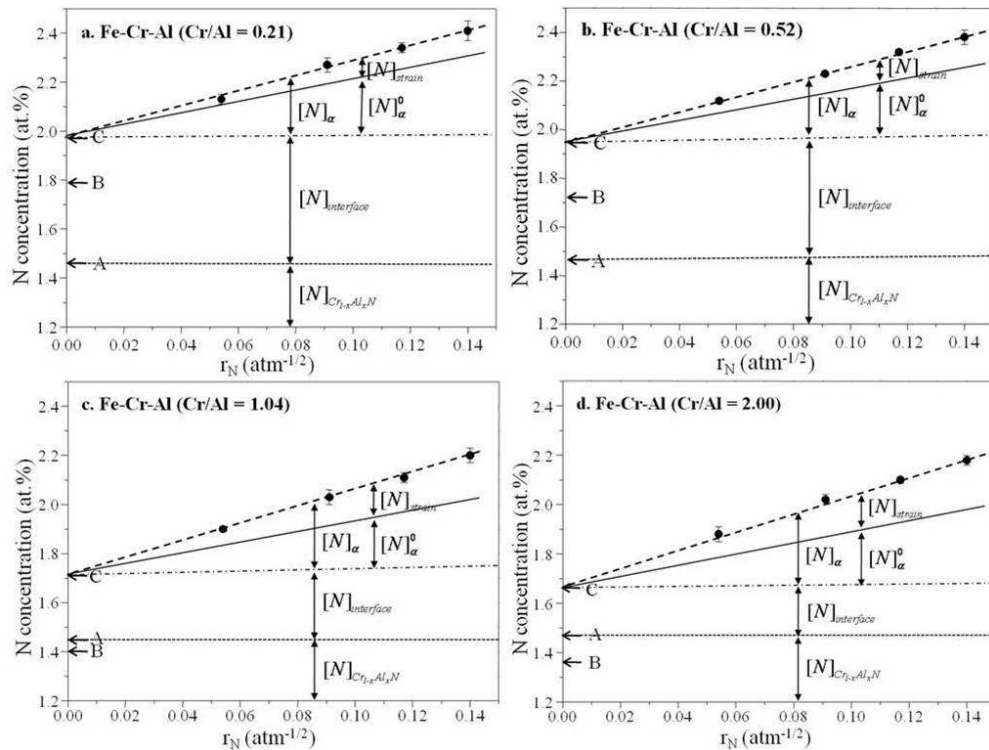


Fig5
174x160mm (149 x 121 DPI)

View Only

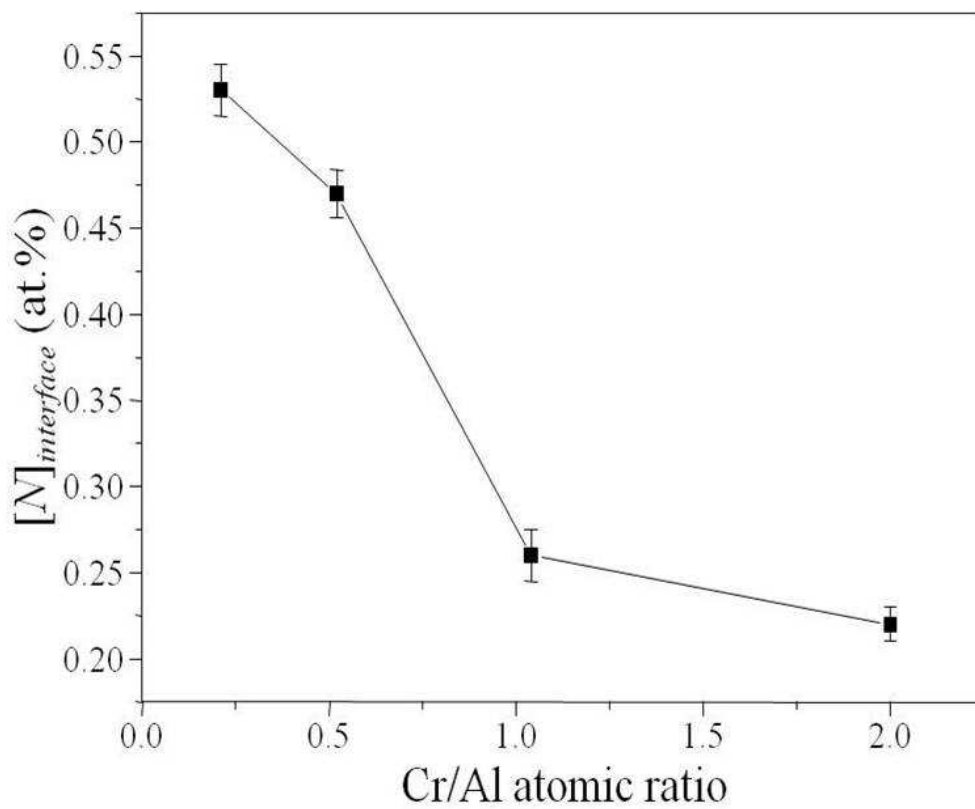


Fig6
129x107mm (150 x 145 DPI)

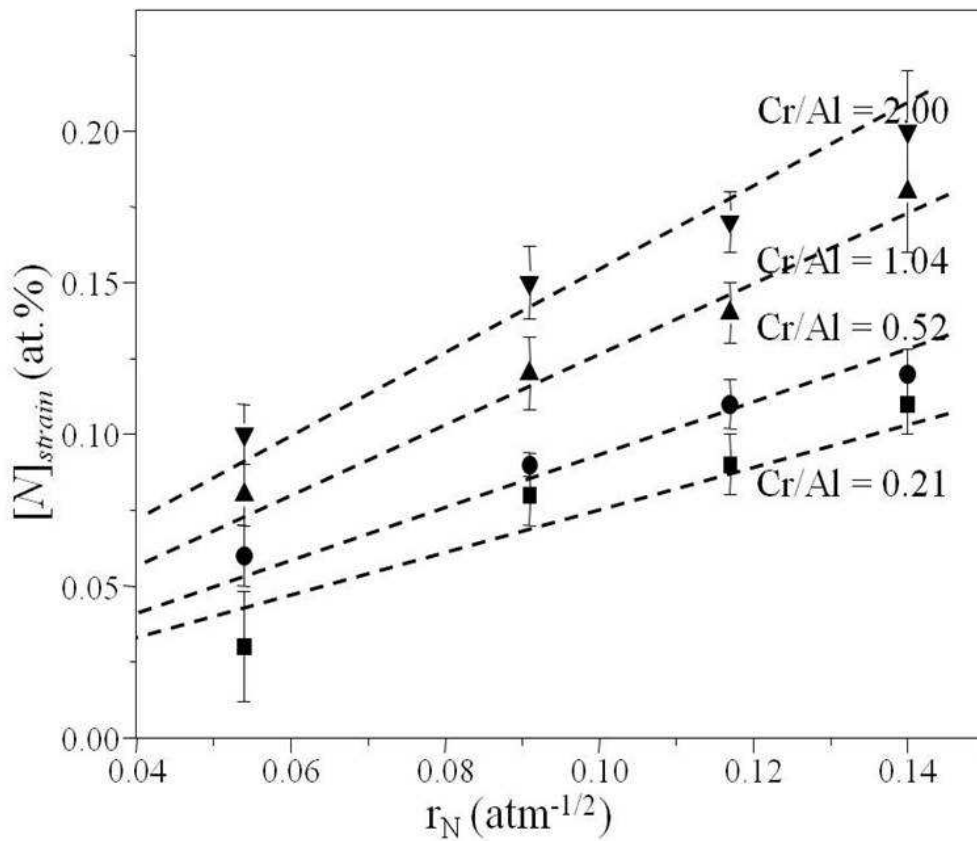


Fig7
129x107mm (150 x 150 DPI)

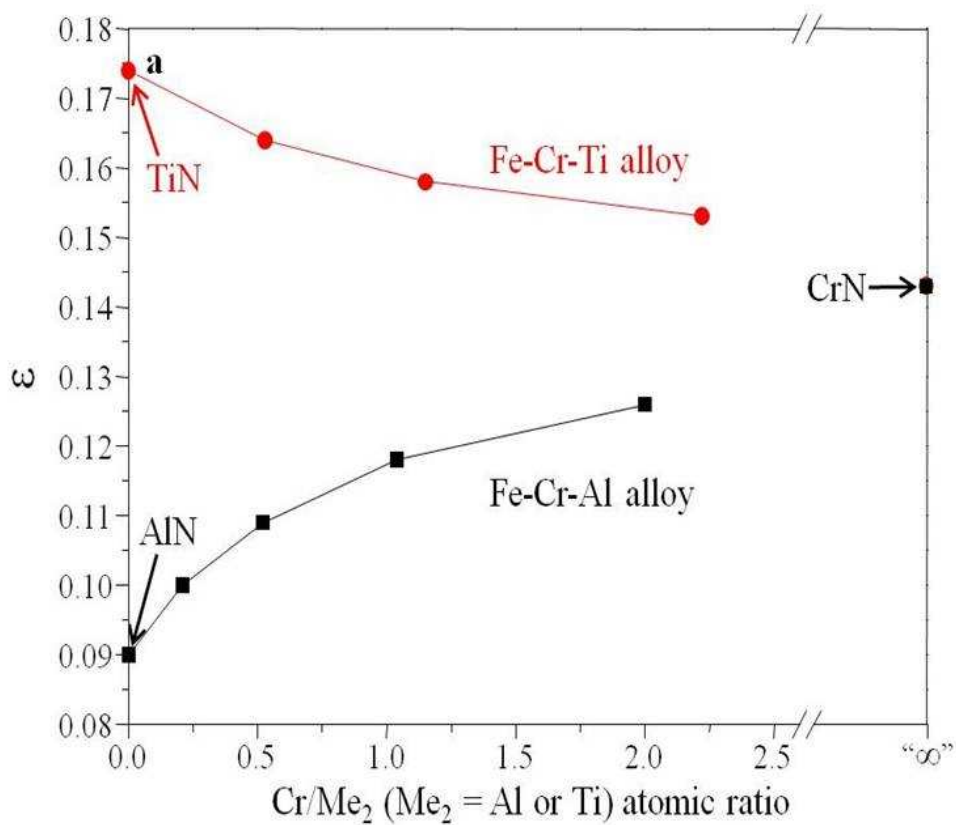


Fig8a
129x107mm (150 x 150 DPI)

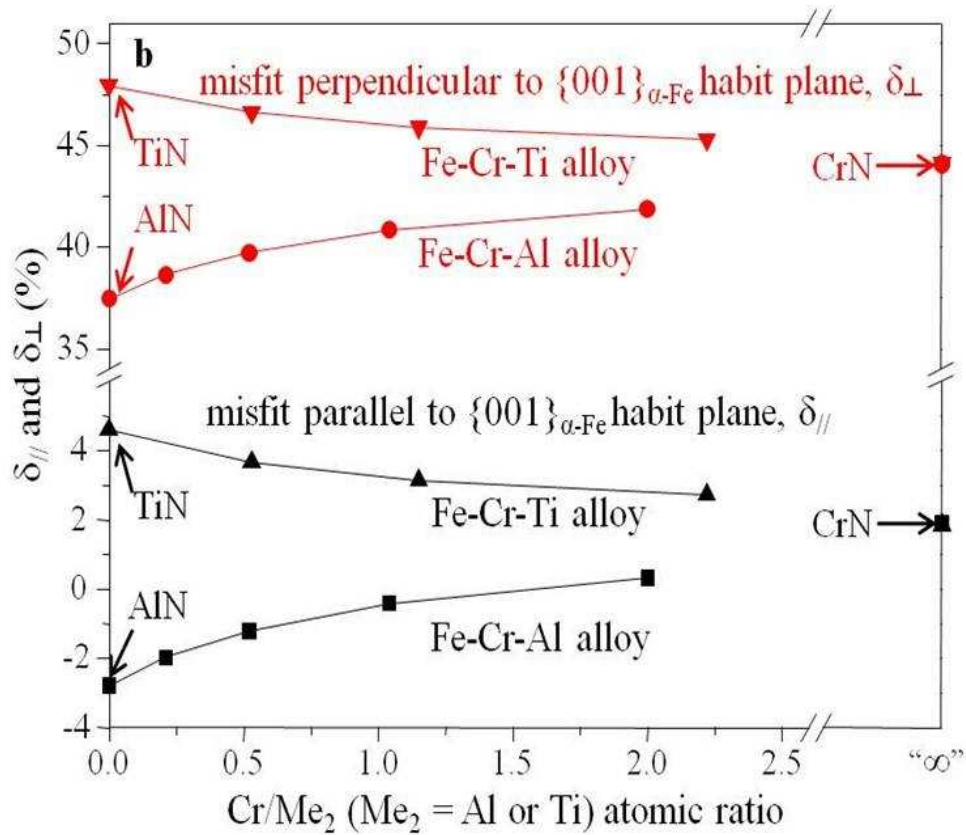


Fig8b
129x107mm (150 x 150 DPI)